Available online at www.sciencedirect.com

ScienceDirect

IFAC Papers Online CONFERENCE PAPER ARCHIVE

IFAC-PapersOnLine 49-1 (2016) 035–040

Enhanced Energy Harvesting from Nonlinear Oscillators via Chaos Control

Aravind Kumar[1] * **Shaikh Faruque Ali**[2] * **Arockiarajan. A**[3] *

* *Department of Applied Mechanics, Indian Institute of Technology Madras, Chennai - 600 036, India.*

[1] *e-mail: aravindkumarerode@gmail.com* [2] *e-mail: sfali@iitm.ac.in*

[3] *e-mail: aarajan@iitm.ac.in*

Abstract: Modern electronic devices require less energy on-board and could be powered by energy harvested from the environment. Broadband vibration energy harvesting is one of the widely explored options for powering such devices. One such harvester that exploits this technique is the nonlinear inverted elastic pendulum. This system has a double-well potential and can undergo large amplitude inter-well oscillations. Piezoelectric patches, pasted near the base of the beam, convert these mechanical oscillations into electrical energy. However, the large amplitude responses can deteriorate over time into low energy chaotic oscillations, thereby reducing the harvested power. Under such conditions, forcing the system to follow a high energy orbit would improve the energy harvested from the system. However, it is not wise to invest a large control force to stabilize the high energy orbits. This manuscript aims to exploit the chaotic nature of the system to stabilize the unstable periodic orbits. The chaotic behavior of the system allows even small perturbations to alter its response dramatically. Taking advantage of this property, a low power controller, based on the method of Ott, Grebogi, and Yorke (OGY), is used to stabilize the unstable high energy periodic orbits. The control strategy is implemented on the linearized system, about the operating point corresponding to the chosen orbit. LQR is used to determine the optimum control force. The devised strategy is numerically simulated, which favors the implementation of OGY control to improve their energy harvesting capabilities.

Keywords: Chaos control; OGY control; Unstable periodic orbits; LQR; Broadband energy harvesting; Vibrations.

1. INTRODUCTION

The realm of wireless devices is witnessing an exponential growth ever since its inception. But a common setback to the extent of services rendered by these devices is the limited lifetime of batteries powering them. Presence of a self-sustainable power source would thus help us to exploit such devices exhaustively. Due to the current technological revolution, devices continue to shrink and less energy is required on-board. This has invoked the interest of researchers to efficiently harvest even a small amount of electrical energy available in the environment. Ambient vibrations, temperature gradients and radiations are some of the sources from which electrical energy could be harvested. Among these, low frequency mechanical vibrations (1-100 Hz) are commonly available and could act as a long term source of power for miniature devices.

The classical design of a vibration energy harvester consists of a cantilever beam carrying a tip mass. This model exploits the linear resonance of the system and uses a transducer to convert mechanical vibrations to electrical energy (Inman and Erturk, 2011). Ambient vibrations are random in nature and under such excitations, the efficiency of resonant harvesters is drastically reduced (Ali et al., 2010). Hence, modern research focuses on broadband energy harvesting where the harvester gives a fairly good output over a broad range of frequencies.

Various broadband harvester designs have been proposed based on nonlinear structural systems in the past decade (Gammaitoni et al., 2009; Erturk et al., 2009; Friswell et al., 2012; Kumar et al., 2015). The key aspect of the nonlinear harvesters is the use of a double well potential, so that the device will have two stable equilibrium positions. Erturk et al. (2009); Stanton et al. (2010) and Masana and Daqaq (2011) highlighted the advantages of a double well potential for energy harvesting, particularly when inter-well dynamics are excited. The simplest equation of motion with a double well potential is the well-known Duffing oscillator. The dynamics is complex, sometimes with coexisting periodic solutions and sometimes exhibiting a chaotic response. The Duffing oscillator model has been used for many energy harvesting systems along with electromechanical coupling for the harvesting circuit.

Favorable bistable harvester behavior involves steady-state large amplitude inter-well oscillations (Friswell et al., 2012). Unfortunately, overlapping dynamic attractors can result in low energy chaotic oscillations for matching excitation criteria (Harne and Wang, 2013; Daqaq et al., 2014). Harvesting can be improved during the low energy chaotic motion by forcing the system to follow a high energy periodic orbit (Geiyer and Kauffman, 2015). However, it is also not wise to invest a large control force to stabilize the high energy orbits.

10.1016/j.ifacol.2016.03.025

Chaotic systems display extreme sensitivity to initial conditions, thus allowing small perturbations to alter their behavior dramatically. In a chaotic attractor, stretching and folding of the trajectories in time give rise to a theoretically infinite number of unstable periodic orbits existing within a bounded region of the state space. Ott et al. (1990) theorized that by using only small parameter perturbations it is possible to stabilize these unstable periodic orbits present in a chaotic attractor. This perturbation method of controlling chaos is since known as the OGY (Ott, Grebogi and Yorke) method.

In this manuscript, an attempt has been made to enhance the energy harvesting capabilities of inverted beam harvester proposed by Friswell et al. (2012) through OGY control. The control input for the system has been optimized based on LQR technique. Numerical simulations are performed to validate the efficacy of the proposed method.

The content of this manuscript is organized as follows. A concise mathematical background of OGY control is presented in Section 2. Section 3 provides a brief description of the inverted elastic pendulum energy harvester and its modeling. The discussions are then extended to design a LQR controller to stabilize the unstable periodic orbits in the harvester in Section 4. Section 5 deals with the numerical simulations carried out to validate the concept. Conclusions are drawn in Section 6.

2. CHAOS CONTROL: MATHEMATICAL BACKGROUND

The prime motive behind application of control to a system is to regulate its behavior as desired. The presence of chaos in physical systems has been extensively demonstrated. However, in practical applications, a system is expected to behave in an ordered fashion. Hence, chaos is strictly avoided from an application standpoint. On the other hand, flexibility is an important property inherently present in chaotic systems that makes us appreciate chaotic motion. A chaotic trajectory is extremely sensitive to the effect of perturbations. Hence, a small perturbation applied at the right time is sufficient to change the system's trajectory and guide it along the desired path. Thus, flexibility of a chaotic system rules out the need for the application of a large control force to drive it to the desired operating point in a brute force manner. Instead, it makes possible to let the system fluctuate and eventually change its dynamics as little as possible to reach the desired state (Macau et al., 2008).

The concept of chaos control came about when Ott et al. (1990) theorized that it is possible to stabilize unstable periodic orbits present in a chaotic system through small, tailored, time-specific parameter perturbations. Also, the flexibility of the chaotic system makes it possible to stabilize different orbits, depending on the situation, in real-time. In the context of energy harvesting, this is very useful in real-time stabilization of a large amplitude orbit that is accessible from a wide range of excitation frequencies, thus enhancing the broadband capabilities of the harvester.

The first step in chaos control is the visualization of the chaotic attractor and the underlying unstable periodic orbits. A Poincare section is helpful in visualizing a chaotic system. Poincare sections (for example, refer Figs. (3&4)) are created from periodic sampling of the system response, with the sampling frequency being equal to the excitation frequency. Hence, each successive point in the Poincare section represents the state that is one period later in time.

Consider a dynamical system as described by (1):

$$\dot{\boldsymbol{X}} = f(\boldsymbol{X}) \tag{1}$$

where $\boldsymbol{X} \in \Re^n$ is the state vector.

A Poincare map relates the state of a dynamical system at any instant to another instant that is one period later in time. Hence, mathematically, a Poincare section can be described as (Strogatz, 2001):

$$\boldsymbol{X_{k+1}} = \boldsymbol{F}(\boldsymbol{X_k}) \tag{2}$$

where k and $k+1$ denote time instances one period apart.

When the response of a conservative system is periodic, a point $\boldsymbol{P^*}$ in the Poincare map maps onto itself the next period. Hence, essentially the Poincare section in this case is a single point. But, during chaotic motion, the motion is non-repetitive. Hence, the existence of a dense set of points in the Poincare section indicates the presence of a chaotic behavior. These dense set of points represent the strange attractor (or) the chaotic attractor of the system. This strange attractor is the bounded structure on which the unstable periodic orbits lie. Hence, isolation of unstable periodic orbits may be done by inspection of the underlying data used to plot the Poincare section.

Let $\boldsymbol{X^*}$ ($\in \Re^n$) be the desired operating point in the Poincare map that corresponds to the chosen orbit. The effectiveness of OGY technique lies in choosing an orbit that has high energy. Let u ($\in \Re^1$) be the control force required to control the dynamical system about the desired operating point $\boldsymbol{X^*}$. The state equation and Poincare section are given by:

$$\dot{\boldsymbol{X}} = f(\boldsymbol{X}, u) \tag{3}$$

$$\boldsymbol{X_{k+1}} = \boldsymbol{F}(\boldsymbol{X_k}, u_k) \tag{4}$$

Typically in a chaotic system, in the absence of a control force, the point $\boldsymbol{X^*}$ maps onto some other point the next period. But the purpose of control force is to make the point $\boldsymbol{X^*}$ map onto itself during the next period, thus stabilizing the periodic orbit that passes through $\boldsymbol{X^*}$. Since the point $\boldsymbol{X^*}$ maps onto itself, it acts as a stable fixed point of the controlled system. Hence,

$$\boldsymbol{X^*} = \boldsymbol{F}(\boldsymbol{X^*}) \tag{5}$$

Let $\boldsymbol{X_k}$ be the state of the system at some instant. Then, the difference between the current state and the fixed point is given as,

$$\boldsymbol{e_k} = \boldsymbol{X_k} - \boldsymbol{X^*} \tag{6}$$

One period later, the difference can be given as,

$$\boldsymbol{e_{k+1}} = \boldsymbol{X_{k+1}} - \boldsymbol{X^*} \tag{7}$$

Substituting (4) and (5) in (7), we get,

$$\boldsymbol{e_{k+1}} = \boldsymbol{F}(\boldsymbol{X_k}, u_k) - \boldsymbol{F}(\boldsymbol{X^*}) \tag{8}$$

$$\boldsymbol{e_{k+1}} = \boldsymbol{F}(\boldsymbol{X^*} + \boldsymbol{X_k} - \boldsymbol{X^*}, u_k) - \boldsymbol{F}(\boldsymbol{X^*}) \tag{9}$$

On expanding up to first order approximation using Taylor Series, we get,

$$\boldsymbol{e_{k+1}} = \left.\frac{\partial \boldsymbol{F}}{\partial \boldsymbol{X}}\right|_{\boldsymbol{X}=\boldsymbol{X^*}} (\boldsymbol{X_k} - \boldsymbol{X^*}) + \left.\frac{\partial \boldsymbol{F}}{\partial u}\right|_{\boldsymbol{X}=\boldsymbol{X^*}} (u_k - 0) \tag{10}$$

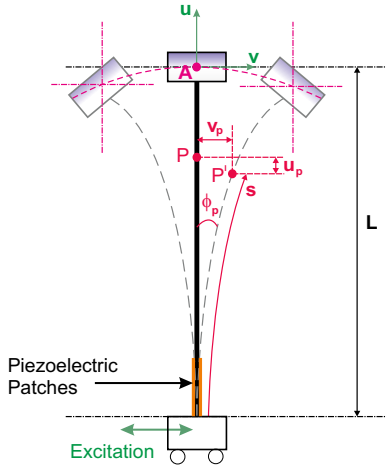

Fig. 1. Inverted Pendulum Energy Harvester: Schematic Representation

Hence,

$$\boldsymbol{e_{k+1}} = \boldsymbol{A}\boldsymbol{e_k} + \boldsymbol{B}u_k \tag{11}$$

$$\text{where, } \boldsymbol{A} = \left.\frac{\partial \boldsymbol{F}}{\partial \boldsymbol{X}}\right|_{\boldsymbol{X}=\boldsymbol{X}^*} \text{ and } \boldsymbol{B} = \left.\frac{\partial \boldsymbol{F}}{\partial u}\right|_{\boldsymbol{X}=\boldsymbol{X}^*}$$

Equation (11) describes the error dynamics of the controlled system in the form of a map. This control form will be used to apply the control force u once per period of excitation of the oscillating system. On successful establishment of control, during every period of oscillation, the states in close vicinity of the operating point $\boldsymbol{X}^*$ collapse onto itself. Hence, the orbit passing through the operating point is stabilized.

The control algorithm given by (11) is applied to a nonlinear energy harvester to enhance its harvesting capabilities. Modeling of the nonlinear harvester and implementation of control are discussed in the subsequent sections.

3. INVERTED ELASTIC PENDULUM HARVESTER

The schematic of an inverted elastic pendulum harvester is shown in Fig. 1. The harvester consists of an inverted Euler-Bernoulli beam carrying a tip mass and is excited at the base. Piezoelectric patches are placed at the base of the beam, in a bimorph configuration, to convert mechanical vibrations into electrical energy. The displacement-curvature relation of the beam is nonlinear due to the large transverse displacement of the beam.

Figure 1 shows the harvester being subjected to a harmonic base excitation $z(t) = z_0 \cos \omega t$. The governing differential equation of motion of the harvester has been derived by Friswell et al. (2012) by assuming a single-mode approximation. A brief review of the formulation is presented here.

Owing to the single-mode approximation, the transverse displacement at any point in the beam can be represented as a function of tip mass displacement v through a function for the beam deformation as (Friswell et al., 2012):

$$v_p(s,t) = v_p(L,t)\psi(s) = v(t)\psi(s) \tag{12}$$

The displacement profile $\psi(s)$ was taken to be (Friswell et al., 2012):

Table 1. Parameters used for Simulation

Elastic Beam		**Piezoelectric Patches**	
Parameters	Values	Parameters	Values
ρ	7850 kg/m^3	L_c	28 mm
E	210 GPa	w_c	14 mm
w	16 mm	h_c	300 μ m
h	0.254 mm	γ_c	-4 $\times 10^{-5}$ Nm/V
L	300 mm	C_p	51.4 nF
M_t	10.5 g	R_l	0.1 MΩ
I_t/M_t	40.87 mm^2		
ζ	0.01		

$$\psi(s) = \lambda_t\left(1 - \cos\left(\frac{\pi s}{2L}\right)\right) \tag{13}$$

where λ_t is a constant such that $\psi(\lambda_t) = 1$.

The kinetic and potential energies of the system were computed and substituted in the Euler - Lagrange equation to obtain the mechanical governing equation. The equation of motion is given as (Friswell et al., 2012):

$$\begin{aligned}\left[\rho A N_1 + M_t + I_t N_5^2 + (\rho A N_3 + M_t N_4^2 + I_t N_5^4)v^2\right]\ddot{v} \\ + \left(\rho A N_3 + M_t N_4^2 + I_t N_5^4\right)v\dot{v}^2 + c\dot{v} \\ + \left[EIN_6 - M_t g N_4 - \rho A g N_9 + 2EIN_7 v^2\right]v \\ - \Theta_1 V - \Theta_2 v^2 V = -(\rho A N_2 + M_t)\ddot{z}\end{aligned} \tag{14}$$

The constants N_1 to N_9, mentioned in Eq.(14), depend on the deformation function of the beam. Please refer Friswell et al. (2012) for a detailed explanation.

In the electrical domain, the governing differential equation has been derived by considering the piezoelectric patches as a capacitor connected in parallel across the load resistance and is given by (Friswell et al., 2012),

$$C_p\dot{V} + \frac{V}{R_l} + \Theta_1\dot{v} + \Theta_2 v^2\dot{v} = 0 \tag{15}$$

where R_l is the load resistor and C_p is the capacitance of the piezoelectric patches. Equations (14) and (15) together represent the dynamics of the system.

4. IMPLEMENTATION OF CONTROL STRATEGY

To begin with, the presence of chaotic oscillations in the inverted elastic pendulum harvester is demonstrated. Subsequently, the design of an LQR controller to stabilize the unstable periodic orbits in the chaotic attractor is discussed.

4.1 Chaos in Inverted Elastic Pendulum Harvester

The inverted elastic pendulum oscillator follows a modified form of Duffing equation wherein geometric nonlinearities are also included. For discussions in this manuscript, the parameters used by Friswell et al. (2012) have been adopted and are shown in Table 1.

The harvester is numerically simulated using MATLAB®. Chaotic oscillations are observed at an excitation amplitude of 16 mm and frequency of 0.5 Hz. The simulated time histories of displacement and voltage are shown in Fig. (2). The corresponding two-dimensional phase portrait between tip mass displacement and velocity along with the

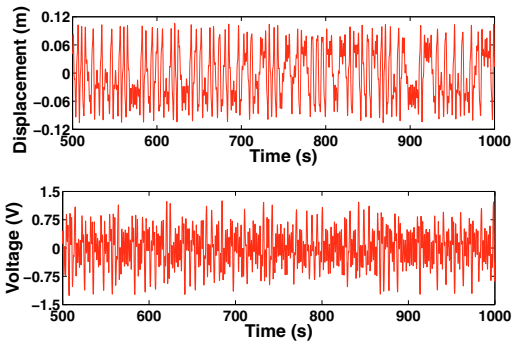

Fig. 2. Time histories of tip mass displacement and generated voltage

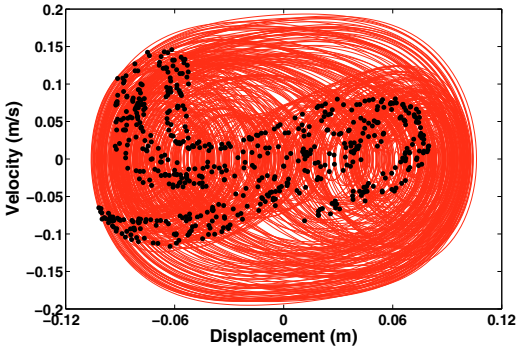

Fig. 3. Phase portrait between tip mass displacement and velocity. The black dots represent the corresponding Poincare section.

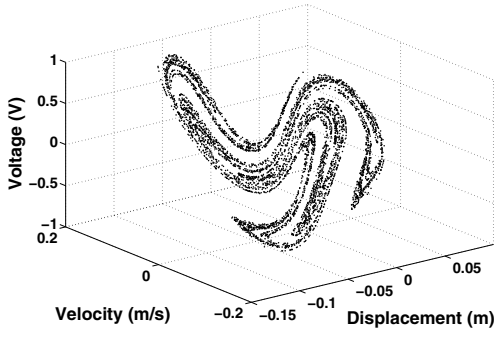

Fig. 4. Poincare section depicting all the three state variables

Poincare section is shown in Fig. (3). The three dimensional Poincare section with all state variables, namely, displacement, velocity and voltage, is shown in Fig. (4). The presence of a dense set of points in the Poincare section indicates the presence of chaos.

The average power harvested per cycle of excitation for the aforementioned parameters is approximately 2.37 μW. An LQR controller is to be implemented to the system to stabilize an unstable periodic orbit so as to increase the harvested power. The design of the LQR controller is described in the following section.

4.2 LQR Control Design

Linear Quadratic Regulator (LQR) technique is a widely used optimal control technique for a linear system. Here, the control force u is minimized based on a quadratic cost function defined as,

$$J = \int_0^\infty \left(\boldsymbol{x}^T \boldsymbol{Q} \boldsymbol{x} + u^T R u \right) \mathrm{d}t \tag{16}$$

Terms $\boldsymbol{Q}$ and R represent a positive definite matrix of order 3×3 and a positive constant respectively. In this case, identity matrix of order 3 is used as $\boldsymbol{Q}$ and $R = 1$.

The feedback control law that minimizes the cost is $u = -\mathbf{K}\mathbf{x}$. Here, $\mathbf{K}$ is the optimal gain matrix, given as $\mathbf{K} = \mathbf{R^{-1}B^{T}P}$. The matrix $\boldsymbol{P}$ is found by solving the continuous time algebraic Riccati equation,

$$\boldsymbol{A^T P} + \boldsymbol{P A} - \boldsymbol{P B R^{-1} B^T P} + \boldsymbol{Q} = 0 \tag{17}$$

With appropriate substitution of variables, $v_1 = v$, $v_2 = \dot{v}$ and $v_3 = V$, the state space representation of the controlled system becomes,

$$\dot{v}_1 = v_2 \tag{18}$$

$$\begin{aligned} \dot{v}_2 = u + \frac{1}{\Delta}\big[&- c v_2 - \left(\rho A N_3 + M_t N_4^2 + I_t N_5^4\right) v_1 v_2^2 \\ &- (EIN_6 - M_t g N_4 - \rho A g N_9) v_1 - 2EIN_7 v_1^3 \\ &+ \Theta_1 v_3 + \Theta_2 v_1^2 v_3 \big] \end{aligned} \tag{19}$$

$$\dot{v_3} = -\frac{v_3}{C_p R_l} - \frac{\Theta_1}{C_p} v_2 - \frac{\Theta_2}{C_p} v_1^2 v_2 \tag{20}$$

where,

$$\Delta = \rho A N_1 + M_t + I_t N_5^2 + (\rho A N_3 + M_t N_4^2 + I_t N_5^4) v_1^2 \tag{21}$$

Here, the control force u is provided through the velocity state equation. The effect of the external excitation is not included in the state space representation but is introduced later in (24).

In a terse form, (18), (19) and (20) can be represented as,

$$\dot{\mathbf{v}} = \mathbf{\Phi}(\mathbf{v}, \mathbf{u}) \tag{22}$$

To apply LQR control strategy, the system dynamics as described by (22) has to be linearized. Let the desired operating point be $\boldsymbol{v_d} = \{v_1^*, v_2^*, v_3^*\}^T$. On linearizing the system about the operating point, we get,

$$\dot{\boldsymbol{x}} = \boldsymbol{A}\boldsymbol{x} + \boldsymbol{B}u \tag{23}$$

where,

$$A = \left.\frac{\partial \mathbf{\Phi}}{\partial \boldsymbol{v}}\right|_{\boldsymbol{v}=\boldsymbol{v}^*} \qquad B = \left.\frac{\partial \mathbf{\Phi}}{\partial u}\right|_{\boldsymbol{v}=\boldsymbol{v}^*}$$

The state vector $\boldsymbol{x}$ in (23) represents the difference between the current state of the system and the operating point. Hence, $\boldsymbol{x} = \boldsymbol{v} - \boldsymbol{v_d}$.

The optimization provided through LQR control holds true for the system described by (23). But in numerical simulations, the effect of external disturbances is also included. Hence, the LQR controller developed in this case is sub-optimal. On substituting $u = -\mathbf{K}\mathbf{x}$ in (23), and adding the effect of external disturbances, we get,

$$\dot{\boldsymbol{x}} = (\boldsymbol{A} - \boldsymbol{B}\boldsymbol{K})\boldsymbol{x} + E\ddot{z} \tag{24}$$

$$\dot{\boldsymbol{x}} = \overline{\boldsymbol{A}}\boldsymbol{x} + E\ddot{z} \tag{25}$$

where, $E = \{0 \;\; -(\rho A N_2 + M_t) \;\; 0\}^T$. The matrix $\overline{\boldsymbol{A}} = \boldsymbol{A} - \boldsymbol{B}\boldsymbol{K}$ is negative definite, thus ensuring that the controlled system is stable.

4.3 Implementation Aspects

The OGY control strategy developed in Section 2 applies to a Poincare map, which is a discrete time representation of the system, with the sampling frequency being equal to the period of oscillations. However, the LQR control algorithm developed in Section 4.2 applies to a continuous time system. Hence, intermittent control has been adopted to convert the developed continuous time control strategy to suit the application. The control force is provided intermittently, only once in a period, with the help of a strategy based on logic. The control force has to be applied whenever the trajectories come within a small region R defined in the neighborhood of the operating point $\mathbf{v}^*$ in the phase space. When the trajectories are outside this region R, the control force has to be zero.

Let $\mathbf{r} = \{r_1\ r_2\ r_3\}^T$ denote the extent of the region R in the neighborhood of the operating point $\mathbf{v}^*$. To make all the states $\boldsymbol{v_k}$ in the region R collapse to the operating point $\mathbf{v}^*$, the maximum control force required would be $u_{max} = -\mathbf{Kr}$. Hence, implementing the following algorithm within the controller would prevent the application of control force outside the region R:

$$u(t) = \begin{cases} 0 & \text{if } |-\mathbf{Kx}(t)| > u_{max} \\ -\mathbf{Kx}(t) & \text{otherwise} \end{cases}$$

Hence, the dynamics of the system is continuous, but the control force applied is made intermittent to comply with the requirements of OGY control.

5. NUMERICAL SIMULATIONS

The developed LQR controller, with due consideration to the implementation aspects discussed in Sec. 4.3, is implemented in the inverted elastic pendulum harvester system and the controlled system is simulated in MATLAB®. The excitation amplitude and frequency are retained as 16 mm and 0.5 Hz respectively. The operating point is chosen as $\{-0.0853\ -0.1859\ -1.227\}^T$. The point is chosen through inspection of the data used for plotting the Poincare section. The extent of control region R is chosen to be $\boldsymbol{r} = \{0.001\ 0.001\ 0.001\}^T$. Control force is applied only when the trajectories come into this region R.

The time histories of the closed loop response of the system and the applied control force are shown in Fig. (5). The corresponding two-dimensional phase portrait between tip mass displacement and velocity along with the Poincare section is shown in Fig. (6). The presence of a single dot in the Poincare section indicates that the motion is periodic. The periodic orbit that is stabilized through the application of control is shown in Fig. (7). The direction of flow along the stabilized orbit is indicated using blue arrows in Fig. (7).

It is obvious from Fig. (7) that the stabilized orbit does not pass through the operating point. This could be explained as follows. The optimal gain obtained form the LQR control strategy for the parameters used is $\boldsymbol{K} = [0.0528\ 6.0375\ 0.0161]$. The feedback gain for velocity is about 100 times greater than that for displacement and voltage. Hence, the effect of velocity dominates in the application of control force. Due to this dominance, the region of control

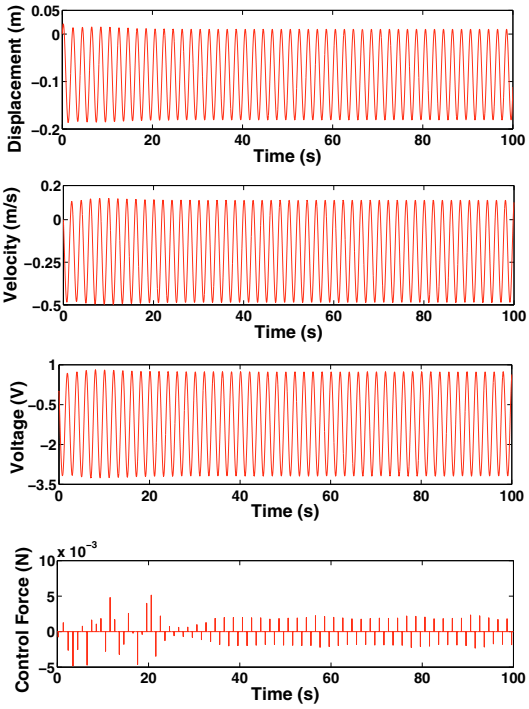

Fig. 5. Time histories of tip mass displacement, velocity, generated voltage and applied control force

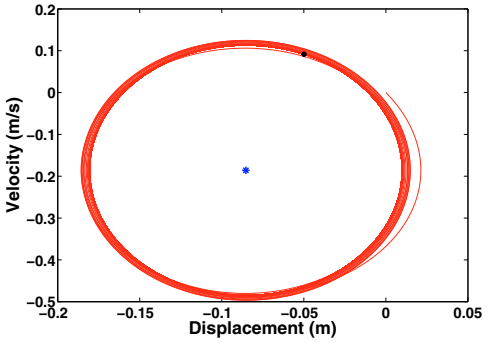

Fig. 6. Phase portrait between tip mass displacement and velocity. The black dots represent the corresponding Poincare section and the blue asterisk represents the operating point.

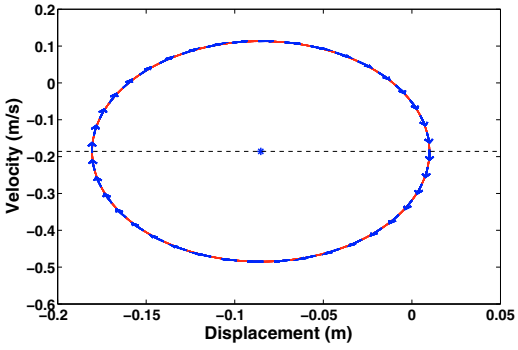

Fig. 7. Phase portrait showing the stabilized orbit. The blue asterisk represents the operating point. Blue arrows represent the direction of flow along the orbit.

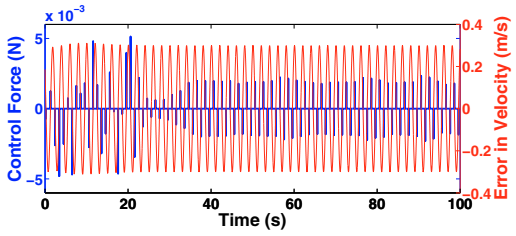

Fig. 8. Relation between error in velocity and control force. The control force is applied whenever the error in velocity approaches zero.

R translates to a small region around the dotted line shown in Fig. (7).

A close examination of the velocity and control force time histories would imply that the control force is applied whenever the error in velocity $x_2 = v_2 - v_2^*$ is close to zero (i.e., within the region R). Thus, the control force is applied twice per period of oscillation, whenever the error in velocity crosses its mean position of zero. Figure 8 provides a more clear picture of this argument.

The average power harvested per cycle of excitation after the implementation of control is approximately 19.09 μW. The limiting value for control force is $u_{max} = -\boldsymbol{Kr} = -0.0061$ N. The limiting value of velocity in the region of control R is 0.001 m/s. Hence, the upper bound for power applied to control the system per cycle of oscillation is $2\times u_{max}\times 0.001 = 12.2\mu$W. Hence, the net power harvested per cycle is 6.89 μW. Thus, the net power harvested increases by a factor of three on implementation of the controller. This proves that the developed control strategy is capable of improving the harvesting capabilities of the harvester. For details regarding the technique used for calculation of power harvested, refer Friswell et al. (2012).

The choice of the operating point affects the power harvested from the harvester. Choosing an operating point corresponding to a higher energy orbit such that the system undergoes inter-well oscillations would enhance the net power harvested.

6. CONCLUSION

An LQR controller has been designed and implemented on an inverted pendulum energy harvester to enhance its harvesting capabilities. Typically, nonlinear energy harvesters give more power when they undergo high amplitude periodic oscillations. But, overlapping dynamic attractors can result in low energy chaotic oscillations for matching excitation criteria. Hence, harvesting improvements during low energy chaotic motion need to be addressed. A controller is developed with an intention to stabilize an unstable high energy periodic orbit and forcing the system to follow it, thus producing more power. The design is based on OGY control theory, which makes use of the flexibility of chaotic motion to control it at the expense of very low power.

The developed controller is numerically simulated. Initial simulations show that the net harvested power increases by a factor of three on implementation of the controller. The effectiveness of the strategy depends on the orbit chosen for stabilization. Choosing a high energy orbit, so that the harvester undergoes inter-well oscillations, would increase the net harvested power. The chosen orbit can also be varied in real-time, so as to suit the operating conditions.

In this manuscript, the control force is applied to the velocity state equation. Alternate methods of application of control force, such as direct control of load resistance, could be explored. This would improve the practical applicability of the developed strategy to energy harvesters. Further, this manuscript shows the possibility of enhancing performance of energy harvesters using chaos control by considering the example of an inverted pendulum energy harvester. However, this does not guarantee the applicability of this method to all other energy harvesters. Feasibility studies must be performed on the concerned harvester before the implementation of this technique.

REFERENCES

Ali, S.F., Friswell, M.I., and Adhikari, S. (2010). Piezoelectric energy harvesting with parametric uncertainty. *Smart Materials & Structures*, 19(10), 105010.

Daqaq, M.F., Masana, R., Erturk, A., and Quinn, D. (2014). On the role of nonlinearities in vibratory energy harvesting: A critical review and discussion. *ASME Applied Mechanics Reviews*, 66(4), 040801.

Erturk, A., Hoffmann, J., and Inman, D.J. (2009). A piezomagnetoelastic structure for broadband vibration energy harvesting. *Applied Physics Letters*, 94, 254102.

Friswell, M.I., Ali, S.F., Bilgen, O., Adhikari, S., Lees, A.W., and Litak, G. (2012). Non-linear piezoelectric vibration energy harvesting from a vertical cantilever beam with tip mass. *Journal of Intelligent Material Systems and Structures*, 23(13), 1505–1521.

Gammaitoni, L., Neri, I., and Vocca, H. (2009). Nonlinear oscillators for vibration energy harvesting. *Applied Physics Letters*, 94, 164102.

Geiyer, D. and Kauffman, J.L. (2015). Chaotification as a means of broadband energy harvesting with piezoelectric materials. *ASME Journal of Vibration and Acoustics*, 137(5), 051005.

Harne, R.L. and Wang, K.W. (2013). A review of the recent research on vibration energy harvesting via bistable systems. *Smart Material Structures*, 22(2), 023001.

Inman, D.J. and Erturk, A. (2011). *Piezoelectric Energy Harvesting*. John Wiley and Sons, Inc., Hoboken, New Jersey.

Kumar, K.A., Ali, S.F., and Arockiarajan, A. (2015). Piezomagnetoelastic broadband energy harvester: Nonlinear modeling and characterization. *The European Physical Journal Special Topics*, 224(14), 2803–2822.

Macau, Elbert, E.N., and Grebogi, C. (2008). *Controlling Chaos*, 1–28. Wiley-VCH Verlag GmbH & Co. KGaA.

Masana, R. and Daqaq, M.F. (2011). Relative performance of a vibratory energy harvester in mono- and bi-stable potentials. *Journal of Sound and Vibration*, 330, 6036–6052.

Ott, E., Grebogi, C., and Yorke, J.A. (1990). Controlling chaos. *Physical Review Letters*, 64(11), 1196–1199.

Stanton, S.C., McGehee, C.C., and Mann, B.P. (2010). Nonlinear dynamics for broadband energy harvesting: Investigation of a bistable piezoelectric inertial generator. *Physica D*, 239, 640–653.

Strogatz, S.H. (2001). *Nonlinear Dynamics and Chaos: With Applications to Physics, Biology, Chemistry and Engineering*, volume 272. Westview Press, Colorado.